

Review

A Review of the Design and Performance of Catalysts for Hydrothermal Gasification of Biomass to Produce Hydrogen-Rich Gas Fuel

Kapil Khandelwal¹, Philip Boahene¹, Sonil Nanda²  and Ajay K. Dalai^{1,*}

¹ Department of Chemical and Biological Engineering, University of Saskatchewan, Saskatoon, SK S7N 5A9, Canada; kak368@mail.usask.ca (K.K.); peb225@mail.usask.ca (P.B.)

² Department of Engineering, Faculty of Agriculture, Dalhousie University, Truro, NS B2N 5E3, Canada; sonil.nanda@dal.ca

* Correspondence: ajay.dalai@usask.ca

Abstract: Supercritical water gasification has emerged as a promising technology to sustainably convert waste residues into clean gaseous fuels rich in combustible gases such as hydrogen and methane. The composition and yield of gases from hydrothermal gasification depend on process conditions such as temperature, pressure, reaction time, feedstock concentration, and reactor geometry. However, catalysts also play a vital role in enhancing the gasification reactions and selectively altering the composition of gas products. Catalysts can also enhance hydrothermal reforming and cracking of biomass to achieve desired gas yields at moderate temperatures, thereby reducing the energy input of the hydrothermal gasification process. However, due to the complex hydrodynamics of supercritical water, the literature is limited regarding the synthesis, application, and performance of catalysts used in hydrothermal gasification. Hence, this review provides a detailed discussion of different heterogeneous catalysts (e.g., metal oxides and transition metals), homogeneous catalysts (e.g., hydroxides and carbonates), and novel carbonaceous catalysts deployed in hydrothermal gasification. The article also summarizes the advantages, disadvantages, and performance of these catalysts in accelerating specific reactions during hydrothermal gasification of biomass, such as water–gas shift, methanation, hydrogenation, reforming, hydrolysis, cracking, bond cleavage, and depolymerization. Different reaction mechanisms involving a variety of catalysts during the hydrothermal gasification of biomass are outlined. The article also highlights recent advancements with recommendations for catalytic supercritical water gasification of biomass and its model compounds, and it evaluates process viability and feasibility for commercialization.

Keywords: biofuels; biomass; catalysts; cellulose; gasification; hemicellulose; hydrogen; lignin; methane; supercritical water



Citation: Khandelwal, K.; Boahene, P.; Nanda, S.; Dalai, A.K. A Review of the Design and Performance of Catalysts for Hydrothermal Gasification of Biomass to Produce Hydrogen-Rich Gas Fuel. *Molecules* **2023**, *28*, 5137. <https://doi.org/10.3390/molecules28135137>

Academic Editor: Dimitrios Kalderis

Received: 15 May 2023

Revised: 28 June 2023

Accepted: 29 June 2023

Published: 30 June 2023



Copyright: © 2023 by the authors. Licensee MDPI, Basel, Switzerland. This article is an open access article distributed under the terms and conditions of the Creative Commons Attribution (CC BY) license (<https://creativecommons.org/licenses/by/4.0/>).

1. Introduction

Owing to increased growth in the population as well as urban and industrial development, global energy consumption has witnessed a dramatic rise over the years. Currently, 80% of the global energy demand is met by fossil fuels such as coal, natural gas, gasoline, and diesel. It cannot be denied that fossil fuels have long-term adverse effects on the environment and ecosystems, including global warming, an increase in greenhouse gas emissions, acid rain, and changes in weather patterns, to name a few [1]. On a global scale, CO₂ emissions from the usage of fossil fuels such as coal, crude oil, and natural gas amount to 15, 12, and 8 billion tons, respectively [2]. Gradually phasing away from fossil fuels and seeking alternative and renewable sources of energy are urgently required.

Biofuels produced from renewable sources such as lignocellulosic biomass, livestock manure, microalgae, municipal solid waste, and sewage sludge are desirable alternatives to fossil fuels for meeting future energy demands and reducing carbon emissions [3,4].

Hydrogen (H_2) has proven to be a clean alternative source to fossil fuels for meeting energy demands because of its zero carbon emissions, higher heating value of 140 MJ/kg, and adiabatic flame temperature of approximately 2100 °C. The combustion products of H_2 are water and heat energy, compared to the combustion of fossil fuels which emits greenhouse gases such as CO_2 , CO, CH_4 , SO_x , and NO_x . In addition to being considered the fuel of the future, hydrogen is also utilized in a wide variety of commercial applications such as fuel cells, upgrading crude oil, synthesis of fine chemicals, metallurgy, pharmaceuticals, and the aerospace industry [5]. A main advantage of H_2 is its ability to produce clean electricity through fuel cells [6]. H_2 is also a valuable precursor in the production of various commodity and specialty chemicals, such as methanol, ammonia, alcohol, and aldehydes, through various catalytic and non-catalytic thermochemical conversion processes [7,8]. H_2 is also extensively used by refineries in hydrotreating processes such as hydrodeoxygenation [9], hydrodenitrogenation [10], hydrodesulfurization [10], and hydrodemetallization [11] to upgrade crude oil and bio-oil to transportation-grade fuels. The sustainable nature of H_2 and its increasing demand in many industrial and commercial sectors has entrenched it as an integral component of the circular economy.

Although hydrogen gas has no color, its production routes have designated it different colors categorization. Hydrogen can be categorized as brown, grey, blue, green, pink, yellow, turquoise, and white based on its production from a wide variety of sources and technologies (Figure 1). Based on the source and production technology employed, hydrogen can be classified into different colors such as brown H_2 (gasification of coal), grey H_2 (steam reforming of methane), blue H_2 (steam reforming of methane with carbon capture), green H_2 (electrolysis using electricity from renewables), pink H_2 (electrolysis using electricity from nuclear energy), turquoise H_2 (methane pyrolysis), yellow H_2 (electrolysis using electricity from solar power), and white H_2 (geological H_2 in underground deposits) [12].



Figure 1. Different color shades of the hydrogen spectrum.

Currently, the major route for the synthesis of H_2 is the steam reforming of methane, which contributes to approximately 95% of global H_2 production [13]. Nearly 250,000 standard cubic feet of CO_2 is emitted per 1 million standard cubic feet of H_2 produced from the steam reforming of CH_4 [14]. Despite the significantly larger carbon footprint of the steam reforming of methane process, it is still commercially applied today. Although not widely commercialized, several sustainable pathways for hydrogen production from alternative

sources are also available, such as electrolysis, photocatalysis, hydrothermal gasification, dark fermentation, and photo-fermentation [15].

The hydrothermal gasification conversion route is capable of sustainably producing H_2 via renewable lignocellulosic biomass sources. This process utilizes water at either subcritical or supercritical conditions as a green solvent and reaction medium to disintegrate complex organic substrates to gases such as H_2 , CH_4 , CO , and CO_2 [16]. When the temperature and pressure of water exceed its critical points of $374\text{ }^\circ\text{C}$ and 22.1 MPa , respectively, supercritical water (SCW) is generated [17]. On the other hand, water is transformed into subcritical water when the temperature and pressure of water are slightly below or near its critical points.

SCW experiences a significant change in its properties compared to liquid water at room conditions, imparting unique properties such as faster kinetics, a non-polar nature, and excellent solubility of gaseous molecules with the absence of interphase transfer boundaries [18,19]. Due to these versatile properties, supercritical water gasification (SCWG) can convert recalcitrant feedstocks with high moisture content into gaseous fuels enriched with combustible gases such as H_2 and CH_4 . SCWG also does not require biomass drying because of its aqueous reaction medium, making the process energy efficient [20]. Due to these advantages, SCWG has recently gained popularity as an environmentally friendly process to produce H_2 from waste feedstocks.

The main products of SCWG are gases (e.g., H_2 , CO , CO_2 , CH_4 , and C_{2+}), hydrochar, and liquid effluents. Hydrochar is a carbon-rich solid product resulting from depolymerization, dehydrogenation, decarboxylation, deamination, and aromatization of the organic feedstock used in SCWG [21]. Further activation and functionalization of hydrochar can enhance its surface area and properties for a wide variety of applications, such as solid fuel, adsorbent, catalyst support, activated carbon, carbon sequestration product, reinforcing material for composites, and soil amendment agent [22–24]. The liquid effluents resulting from the hydrothermal decomposition of biomass contain alcohols, furfurals, carboxylic acids, esters, ethers, aliphatics, aldehydes, ketones, and phenolics [25]. Some of these degradation compounds may further polymerize to form tar, which is a challenging component that causes plugging as well as heat and mass transfer limitations in the processors [26]. It should be noted that process conditions such as temperature, reaction time, pressure, and feedstock concentration largely impact the yields and composition of gases, liquids, and hydrochar from the SCWG of biomass [20].

Catalysts also play an important role in improving the process efficiencies of SCWG, especially carbon gasification efficiency and selectivities of gases, by regulating specific reaction mechanisms [27,28]. Several homogeneous and heterogeneous catalysts have been designed and investigated for the SCWG of different biomasses. However, the literature on the application of different catalysts in SCWG appears to be scattered. In addition, in-depth knowledge is scarce on understanding the different reaction pathways, mechanisms, and product properties impacted by homogeneous and heterogeneous catalysts in SCWG. Hence, this review paper attempts to categorically summarize the recent advancements in different homogeneous and heterogeneous catalysts used in SCWG. Furthermore, the challenges and shortcomings of different catalysts are also identified, followed by a discussion and recommendations for the effective design of catalysts, catalytic supports, and promoters used in the SCWG of biomass to produce high-value gaseous fuels.

2. Homogeneous Catalysts Used in Hydrothermal Gasification

Homogeneous catalysts used in SCWG generally consist of alkali metal and hydroxide catalysts. Table 1 summarizes some notable studies on the application of homogeneous catalysts in the SCWG process [29–35]. Homogeneous catalysts promote water–gas shift reactions by favoring C–C bond breakup, thus improving H_2 yields [36]. The water–gas shift reaction results in the formation of H_2 and CO_2 because of the reaction of CO and H_2O . The produced H_2 can further react with the reactive intermediates generated by the catalytic action of homogeneous catalysts to increase overall gas yields [31]. Homogeneous

catalysts usually have rapid conversion rates and can be used in both batch and continuous reactors. Homogeneous catalysts are also cost-effective with negligible sintering [26].

Table 1. Notable studies on SCWG of waste biomass assisted by homogeneous catalysts.

Feedstock	Catalyst	Operating Conditions	Main Findings	Reference
Cellulose and lignin	K ₂ CO ₃	<ul style="list-style-type: none"> • Temperature: 300–600 °C • Reaction time: 1 h • Feed concentration: 7.4 wt% (0.45 M) • Pressure: 9–41 MPa • Reactor: Batch 	<ul style="list-style-type: none"> • K₂CO₃ enhanced gasification efficiency and limited char formation. • The highest H₂ and CH₄ yields were obtained with K₂CO₃ at 600 °C. 	Kang et al. [29]
Cellulose and lignin	K ₂ CO ₃	<ul style="list-style-type: none"> • Temperature: 300–600 °C • Reaction time: 1 h • Pressure: 9–41 MPa • Reactor: Batch 	<ul style="list-style-type: none"> • K₂CO₃ enhanced the water–gas shift reaction, leading to a high H₂ yield. • The highest H₂ yield of 28 mmol/g was achieved with K₂CO₃ at 600 °C from SCWG of glucose. • Total organic carbon levels decreased with catalyst loading, indicating efficient gasification of the feedstock. 	Madenoglu et al. [30]
Glucose	KOH	<ul style="list-style-type: none"> • Temperature: 450–560 °C • Reaction time: 6–10 s • Feed concentration: 0.2–2 wt% • Pressure: 25 MPa • Reactor: Continuous 	<ul style="list-style-type: none"> • The highest heating value of 113% was achieved with KOH catalysts at optimized gasification conditions. 	Garcia-Jarana et al. [31]
Glucose	Raney nickel and K ₂ CO ₃	<ul style="list-style-type: none"> • Temperature: 500 °C • Reaction time: 1 h • Feed concentration: 5 wt% • Pressure: 30 MPa • Reactor: Batch 	<ul style="list-style-type: none"> • 0.5 wt% K₂CO₃ demonstrated better catalytic activity than 1 wt% Raney nickel. 	Snağ et al. [32]
Paper sludge and black liquor	KOH, K ₂ CO ₃ , and NaOH	<ul style="list-style-type: none"> • Temperature: 500–650 °C • Reaction time: 2 min • Feed concentration: 2–3 wt% • Pressure: 25 MPa • Reactor: Semi-continuous 	<ul style="list-style-type: none"> • The highest H₂ yield of 25 mmol/g was obtained with K₂CO₃ at 600 °C from SCWG of paper sludge. 	Rönnlund et al. [33]
Sewage sludge	KOH, K ₂ CO ₃ , NaOH, Na ₂ CO ₃ , and AC	<ul style="list-style-type: none"> • Temperature: 450 °C • Reaction time: 1 h • Pressure: 23–26 MPa • Reactor: Batch 	<ul style="list-style-type: none"> • KOH increased gas yield to 12.2 mmol/g from 11.3 mmol/g in the non-catalytic run. • K₂CO₃ demonstrated the highest desulfurization effect followed by Na₂CO₃, NaOH, KOH, and AC. 	Feng et al. [34]
Timothy grass	KOH, K ₂ CO ₃ , NaOH, and Na ₂ CO ₃	<ul style="list-style-type: none"> • Temperature: 650 °C • Reaction time: 45 min • Biomass-to-water ratio: 1:8 • Pressure: 23–25 MPa • Reactor: Batch 	<ul style="list-style-type: none"> • KOH demonstrated the highest H₂ yield (8.9 mmol/g) followed by K₂CO₃ (7.8 mmol/g), NaOH (6.7 mmol/g), and Na₂CO₃ (6.3 mmol/g). • KOH enhanced the water–gas shift reaction to maximize the H₂ yield. • NaOH enhanced the methanation reaction favoring CH₄ formation at the expense of H₂. 	Nanda et al. [35]

Su et al. [37] reported a base-catalyzed mechanism of alkali metals that enabled the water–gas shift reaction. The degradation intermediates were anions comprising hydroxides, carbonates and formates. Mixing the carbonates in water produced CO₂ and hydroxides. Hydroxides can further combine with CO to produce formate. Further decomposition of formaldehyde can generate H₂. Watanabe et al. [38] reported an ionic-catalyzed mechanism of alkali metals in the SCWG of methanol. They proposed that the ionic species stabilized the methanol by protonation or disassociation. Methanol then oxidized into CO, and protons stabilized the produced CO. CO₂ was formed via the

oxidation of CO, and hydroxide ions favored the water–gas shift reaction to convert CO into CO₂. Thus, the oxidization of CO to CO₂ was enhanced by the hydroxyl ions.

Figure 2 represents a simplified catalytic mechanism of potassium metal in the SCWG of biomass [39]. Sinaž et al. [32] compared K₂CO₃ (a homogeneous catalyst) with Raney nickel (a heterogeneous catalyst) in the SCWG of glucose. Their results showed that the catalytic action of K₂CO₃ enhanced H₂ production while suppressing the formation of phenols for improved gasification efficiency. K₂CO₃ demonstrated superior catalytic activity as compared to Raney nickel. K₂CO₃ showed higher yields of H₂ and CO₂ than Raney nickel, which confirmed its catalytic action to promote the water–gas shift reaction. The catalytic mechanism of K₂CO₃ in enhancing water–gas shift via formate (HCOO[−] K⁺) formation is presented in the following equations. The produced potassium formate further reacts with excess water to generate H₂ with KHCO₃, which decomposes into CO₂ and K₂CO₃.

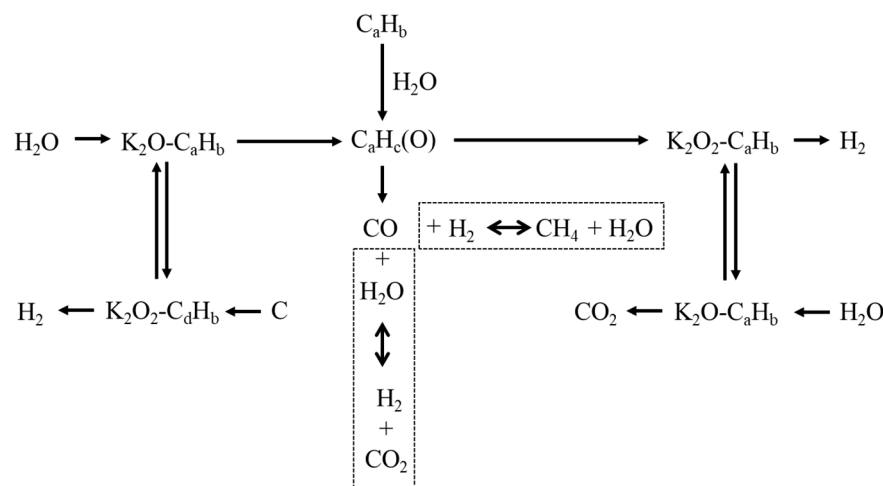


Figure 2. Catalytic mechanism of potassium in SCWG of biomass (adapted with permission from Ge et al. [39]).

Madenoglu et al. [30] studied the kinetics effects of K₂CO₃ in the SCWG of cellulose, lignin, and their mixtures. Their results showed that K₂CO₃ promoted the rates of gasification reactions and prevented the formation of char. Both gas and aqueous phase yields increased at the expense of char yield due to the catalytic effects of K₂CO₃. K₂CO₃ also favored the water–gas shift reaction, thus increasing the H₂ yield.

Sinaž et al. [40] studied the catalytic effect of K₂CO₃ on glucose, phyto-mass (plant residues without proteins), and zoo-mass (meat residues containing proteins). The addition of K₂CO₃ had a significant influence in promoting the water–gas shift reaction during the SCWG of glucose and enhanced H₂ production. However, its catalytic effects in promoting water–gas shift during the SCWG of phyto-mass and zoo-mass were minimal.

Nanda et al. [35] compared four different homogeneous catalysts, Na₂CO₃, K₂CO₃, NaOH, and KOH, in the SCWG of Timothy grass. An increase in catalyst loading from 1% to 3% increased the total gas yield, as well as H₂, CH₄, and CO₂ yields, but decreased the CO yield for all catalysts. This indicated the catalytic action of alkali catalysts promoted gasification efficiency and the water–gas shift reaction. KOH showed the highest H₂ yield of 9 mol/kg, followed by K₂CO₃, NaOH, and Na₂CO₃. A similar trend was observed for total gas yields. The highest total gas and H₂ yields with KOH were explained by

its catalytic action to promote the water–gas shift reaction. On the other hand, NaOH enhanced the methanation reaction with the consumption of H₂, increasing CH₄ yields. Nanda et al. [41] also confirmed the superior catalytic effects of KOH in the SCWG of fructose where KOH showed a higher H₂ yield than NaOH with nearly three times more H₂ yield than non-catalytic reactions.

Yanik et al. [42] compared the activities and selectivities of K₂CO₃, Trona, red mud, and Raney nickel catalysts in the SCWG of cotton stalk, corncob, and tannery wastes. Their results showed that all four catalysts significantly enhanced H₂ yields by favoring water–gas shift and reforming reactions. K₂CO₃ demonstrated the highest H₂ yield with no CO detected in the gas products. However, the catalytic activity of Trona was analogous to that of K₂CO₃. Ferreira-Pinto et al. [43] investigated the effects of NaOH, KOH, and Na₂CO₃ catalysts in the SCWG of lactose. The increase in H₂ yield was highest with NaOH, followed by Na₂CO₃ and KOH. All catalysts inhibited char formation and significantly reduced the total organic carbon content in the reactants, indicating high gasification efficiencies.

Alkali catalysts can also significantly reduce the sulfur content in gas products. High sulfur content in gas products is a serious issue as its combustion can release SO_x. Sulfur can also deactivate and poison the catalysts as well as corrode pipelines. Feng et al. [34] used different homogeneous catalysts (e.g., KOH, K₂CO₃, NaOH, Na₂CO₃, and activated carbon or AC) in the SCWG of sewage sludge. K₂CO₃ showed the best desulfurization effect and limited the H₂S and SO₂ contents to around 140 ppm and 200 ppm, respectively. The order of desulfurization effects of catalysts was found to be: K₂CO₃ > Na₂CO₃ > NaOH > KOH > AC. KOH demonstrated the highest H₂ yield and selectivity. Alkali catalysts converted the unstable sulfur compounds into stable sulfur compounds by promoting cyclization and oxidation reactions, thus preventing the migration of sulfur into gas and liquid products.

Zhong et al. [44] investigated the catalytic performance of KOH, K₂CO₃, KMnO₄, and H₂O₂ on polycyclic aromatic hydrocarbons (PAHs) and gas formation during the SCWG of coking sludge. Their results showed that the PAH content decreased in the catalytic SCWG experiments. The catalytic action of KOH was attributed to its ability to promote free radical reactions during SCWG. These free radicals promote ring-opening reactions of PAHs, leading to their decomposition. KOH led to a higher H₂ yield than K₂CO₃ because of an improved water–gas shift reaction through the formation of a formate intermediate and hydroxyl ions. These hydroxyl ions efficiently capture CO₂ produced from the water–gas shift reaction. This shifted the equilibrium of the water–gas shift reaction towards the products side, thus producing more H₂. Despite the numerous advantages of homogeneous catalysts, they can easily cause reactor plugging and corrosion in the reactor [45]. The recovery of homogeneous catalysts is also difficult compared to that of heterogeneous catalysts, which adds to overall process expenditures [46].

3. Heterogeneous Catalysts Used in Hydrothermal Gasification

Heterogeneous catalysts applied in the SCWG process can be broadly divided into two categories, namely metal oxides and transition metals. The recovery and recycling of heterogeneous catalysts are relatively easier compared to those of homogeneous catalysts [47]. Heterogeneous catalysts are more active, resulting in efficient and improved gasification efficiency [48]. They are also more selective for specific products by promoting desired reactions. A summary of promising studies on the use of heterogeneous catalysts in SCWG is presented in Table 2 [27,49–55].

Table 2. Notable studies on SCWG of waste biomass assisted by heterogeneous catalysts.

Feedstock	Catalyst	Operating Conditions	Main Findings	Reference
2-Propanol	Pt/Al ₂ O ₃ and Ru/Al ₂ O ₃	<ul style="list-style-type: none"> • Temperature: 400–550 °C • Reaction time: 10–30 s • Feed concentration: 0.5 M • Pressure: 25 MPa • Reactor: Continuous 	<ul style="list-style-type: none"> • Pt/Al₂O₃ showed high H₂ selectivity at lower temperatures than Ru/Al₂O₃. • Ru/Al₂O₃ showed 10 mol% H₂ compared to 96 mol% H₂ in the case of Pt/Al₂O₃. • The low H₂ selectivity of Ru/Al₂O₃ was due to enhancement of the methanation reaction, which led to CH₄ yields. 	Karakuş et al. [49]
Glucose	Ni/Al ₂ O ₃ and Ni/CeO ₂ -Al ₂ O ₃	<ul style="list-style-type: none"> • Temperature: 400 °C • Feed concentration: 9.1 wt% • Pressure: 24.5 MPa • Reactor: Batch 	<ul style="list-style-type: none"> • Both catalysts significantly improved the H₂ yield and selectivity. • Ni/CeO₂-Al₂O₃ showed superior catalytic activity than Ni/Al₂O₃ with higher yields of total gases and H₂. • The high activity of Ni/CeO₂-Al₂O₃ was attributed to the inhibition of coke formation and sintering by Ce metal in catalysts. • Further addition of Ce improved the H₂ yield and selectivity, attaining maxima at 8.5 wt% loading. 	Lu et al. [50]; Lu et al. [51]
Glucose	Ni/Al ₂ O ₃ and Ru-Ni/Al ₂ O ₃	<ul style="list-style-type: none"> • Temperature: 400–500 °C • Feed concentration: 45 kg/m³ • Pressure: 25–35 MPa • Reactor: Batch 	<ul style="list-style-type: none"> • Aerogel-synthesized catalysts showed high H₂ yields compared to mesoporous and wet-impregnated catalysts. • The supercritical CO₂ drying step in the aerogel synthesis method enhanced the surface area and reactant diffusivity to improve catalytic performance. • Ru-Ni/Al₂O₃ demonstrated the highest H₂ yield of 4.9 mmol/g. • The high H₂ yield and stability of Ru-Ni/Al₂O₃ were due to the inhibition of graphite coke formation by Ru metal. 	Hossain et al. [52]
Glucose, cellulose, fructose, xylan, pulp, lignin, and bark	Ni/Al ₂ O ₃ , Ni/hydrotalcite, Raney nickel, Ru/C, and Ru/Al ₂ O ₃	<ul style="list-style-type: none"> • Temperature: 380 °C • Reaction time: 15 min • Feed concentration: 2 wt% • Pressure: 25 MPa • Reactor: Batch 	<ul style="list-style-type: none"> • Ni/Al₂O₃ demonstrated the highest H₂ selectivity. • Ni/hydrotalcite showed the highest H₂ yield for all the feedstocks followed by Ni/Al₂O₃. • The high H₂ yield of Ni/hydrotalcite and Ni/Al₂O₃ was attributed to the poor dispersion of Ni metal. 	Azadi et al. [27]
Plastic wastes	NiO/γ-Al ₂ O ₃ , RuO ₂ /γ-Al ₂ O ₃ , and bimetallic catalysts	<ul style="list-style-type: none"> • Temperature: 450 °C • Reaction time: 1 h • Feed concentration: 20 wt% • Pressure: 25 MPa • Reactor: Batch 	<ul style="list-style-type: none"> • The highest carbon gasification efficiency of 99% was achieved with polypropylene followed by high-density polyethylene, low-density polyethylene, and polystyrene. • The highest H₂ yield in the non-catalytic run was achieved with low-density polyethylene followed by polystyrene, polypropylene, and high-density polyethylene. • Compared to only using NiO, the bimetallic catalyst with RuO₂ increased the H₂ yield and reduced C₂–C₄ gas yields. 	Onwudili and Williams [53]

Table 2. Cont.

Feedstock	Catalyst	Operating Conditions	Main Findings	Reference
Soyabean straw	Ni supported on carbon nanotubes (CNT), ZrO ₂ , Al ₂ O ₃ , SiO ₂ , and Al ₂ O ₃ -SiO ₂ , and promoted by K, Ce, and Na.	<ul style="list-style-type: none"> • Temperature: 500 °C • Reaction time: 45 min • Biomass-to-water ratio: 1:10 • Pressure: 23–25 MPa • Reactor: Batch 	<ul style="list-style-type: none"> • Ni supported on ZrO₂ and Al₂O₃ demonstrated superior performance compared to other supports. • 10%Ni-1%Ce/ZrO₂ showed the highest H₂ yield of 10.9 mmol/g and excellent catalytic performance. • This was attributed to the high oxygen storage and mobility capabilities of Ce promoters for high reduction and oxidation performance. 	Okolie et al. [54]
Waste cooking oil	Ru/Al ₂ O ₃ , Ni/Si-Al ₂ O ₃ , K ₂ CO ₃ , and Na ₂ CO ₃	<ul style="list-style-type: none"> • Temperature: 375–675 °C • Reaction time: 15–60 min • Feed concentration: 25–40 wt% • Pressure: 23–25 MPa • Reactor: Batch 	<ul style="list-style-type: none"> • The order of catalytic performance in enhancing the H₂ yield was Ru/Al₂O₃ (10.2 mmol/g) > Ni/Si-Al₂O₃ (9.3 mmol/g) > K₂CO₃ (8.1 mmol/g) > Na₂CO₃ (7.5 mmol/g). • Ru enhanced the water–gas shift reaction to improve H₂ yields. 	Nanda et al. [55]
Wheat straw	Ni/MgO, Fe/MgO, Cu/MgO, Ni/ZnO, Ni/Al ₂ O ₃ , and Ni/ZrO ₂	<ul style="list-style-type: none"> • Temperature: 450 °C • Reaction time: 20 min • Feed concentration: 7.4 wt% • Pressure: 23–28 MPa • Reactor: Batch 	<ul style="list-style-type: none"> • The order of H₂ yield was Ni/MgO (11.6 mmol/g) > Fe/MgO (9.2 mmol/g) > Cu/MgO (8.1 mmol/g). • Among Ni-based supported catalysts, Ni/MgO demonstrated the highest H₂ yields. • Basic supports favored water–gas shift reactions, leading to high H₂ yields. 	Lu et al. [51]

3.1. Transition Metals

3.1.1. Nickel-Based Catalysts

Nickel-based catalysts are the most widely used heterogeneous catalysts in SCWG because of their high activity compared to other expensive transition metal catalysts. Ni-based catalysts require comparatively lower temperatures and promote biomass gasification with higher efficiency. However, Ni-based catalysts can also consume the produced H₂, CO, and CO₂ due to their high methanation activity, producing CH₄ [56]. Furusawa et al. [57] used the Ni/MgO catalyst in the SCWG of lignin. They studied its regenerative capabilities by recovering and reusing the catalyst thrice. The catalyst showed satisfactory regenerative capability before suffering from deactivation due to the formation of carbon and Mg(OH)₂.

Zhang et al. [58] studied the SCWG of glucose and compared the activities and H₂ selectivities of Ni, Co, Ru, and Cu transition metals on γ -Al₂O₃, AC, and ZrO₂ supports. Both 10%Ni/ γ -Al₂O₃ and 10%Ru/Al₂O₃ demonstrated the highest catalytic activities and H₂ selectivities. The order of activity of the supports for the Ni catalyst was: γ -Al₂O₃ > ZrO₂ > AC. Due to satisfactory results with 10%Ni/ γ -Al₂O₃, further enhancement with Na, K, Mg, and Ru promoters was also studied. The addition of the 0.5%K promoter on 10%Ni/ γ -Al₂O₃ significantly increased the H₂ yield by favoring the water–gas shift reaction.

Azadi et al. [28] studied the SCWG of various lignocellulosic feedstocks (e.g., glucose, fructose, cellulose, pulp, xylan, bark, and lignin) using five transition metals catalysts (e.g., Ni/Al₂O₃, Ru/C, Raney nickel, Ni/hydrotalcite, and Ru/Al₂O₃). The activities of Ni/Al₂O₃ and Ni/hydrotalcite catalysts for SCWG demonstrated the highest H₂ selectivities. In contrast, Raney nickel showed the lowest H₂ selectivity. Ni/ α -Al₂O₃ and Ni/hydrotalcite also demonstrated low CH₄ yields at high temperatures and longer reaction times. The high H₂ selectivities of Ni/ α -Al₂O₃ and Ni/hydrotalcite were attributed to the lower nickel dispersion and large crystallite sizes of Ni/ α -Al₂O₃ and Ni/hydrotalcite

catalysts compared to Raney nickel. The high nickel dispersion of Raney nickel strongly favored C–O bond cleavage compared to Ni/Al₂O₃ and Ni/hydrotalcite catalysts, thus explaining the low H₂ selectivity of Raney nickel. The authors also reported that among all feedstocks, lignin was the most resistant to SCWG because of its branched polymeric structure. The lowest gas yield obtained from lignin was attributed to potential deactivation of the catalysts due to its sulfur content.

Azadi et al. [27] compared Ni catalysts on different support materials, including γ -Al₂O₃, α -Al₂O₃, activated carbon, carbon nanotubes (CNT), hydrotalcite, MgO, SiO₂, silica gel, TiO₂, ZrO₂, and various zeolites in the SCWG of glucose. The 20%Ni/ α -Al₂O₃ catalyst showed the highest H₂ selectivity, and Ni/CNT demonstrated high H₂ yields (17–24 mmol/g) and high stability with maximum carbon gasification efficiency. On the other hand, Ni/MgO demonstrated a better H₂ yield (26 mmol/g) and satisfactory carbon gasification efficiency. Due to its low cost and high stability, the authors further investigated the Ni/ α -Al₂O₃ catalyst by varying Ni loading and using promoters. Tin increased the H₂ selectivity but decreased the catalytic activity, whereas alkali promoters increased the carbon gasification efficiency but decreased the H₂ selectivity. Lu et al. [50] also studied Ni-based catalysts with various promoted Al₂O₃ supports (e.g., CeO₂/Al₂O₃, MgO/Al₂O₃, La₂O₃/Al₂O₃, and ZrO₂/Al₂O₃) in the SCWG of glucose. CeO₂/Al₂O₃ showed the highest H₂ yield, followed by La₂O₃/Al₂O₃, ZrO₂/Al₂O₃, Al₂O₃, and MgO/Al₂O₃.

Onwudili and Williams [53] investigated the catalytic SCWG of various plastic wastes with Ru and Ni catalysts. By increasing RuO₂ loading up to 5 wt% in the SCWG of low-density polyethylene, the H₂ yield rose from 1 to 9.9 mol/kg at 450 °C in 1 h. However, the subsequent increase in RuO₂ loading from 5 wt% to 20 wt% decreased the H₂ yield to 4.9 mol/kg while increasing the hydrogen gasification and carbon gasification efficiency. By using a 20 wt% RuO₂- γ -Al₂O₃ catalyst, polypropylene produced a high H₂ yield and the highest carbon gasification efficiency of 99%. High- and low-density polyethylenes also showed similar gas yields, whereas polystyrene produced the lowest yields of C₂-C₄ gases. Low-density polyethylene demonstrated the highest H₂ yield, followed by polystyrene, polypropylene, and high-density polyethylene.

Adamu et al. [59] studied Ce-mesoAl₂O₃ support impregnated with Ni in the SCWG of glucose (Figure 3). Ce-mesoAl₂O₃ had superior support properties compared to γ -Al₂O₃, such as moderate acidity, which helped to reduce coke formation and enabled high metal loading with low agglomeration. The Ni(20)/Ce-Al₂O₃ catalyst exhibited a very high H₂ yield of 10.2 mol/mol of glucose. The meso-form led to the cracking of large intermediates such as tar compounds. Furthermore, Ce helped to improve the thermal stability of the alumina support.

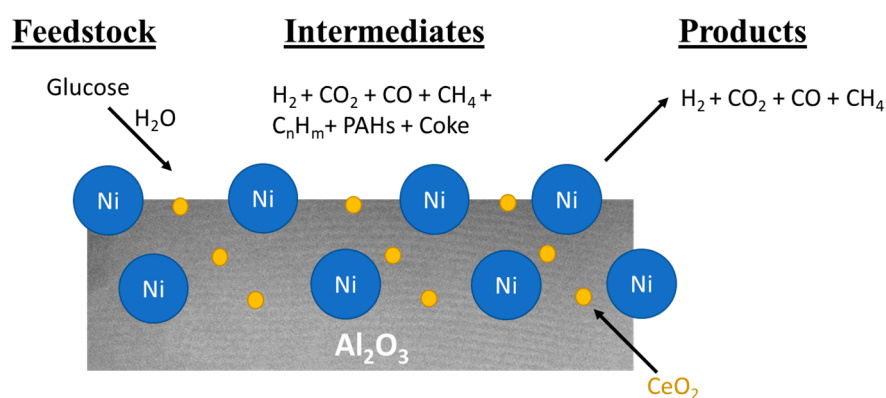


Figure 3. Catalytic mechanism of Ni/Ce-Al₂O₃ in SCWG of glucose (adapted with permission from Adamu et al. [59]).

Lu et al. [51] compared Ni, Cu, and Fe transition metals supported on MgO in the SCWG of wheat straw. The H₂ yields varied with the application of different catalysts in

the following order: Ni/MgO > Fe/MgO > Cu/MgO. Due to excellent H₂ selectivity with Ni, the authors explored various supports, such as basic oxides (MgO and ZnO), acidic oxide (Al₂O₃), and amphoteric oxide (ZrO₂). The H₂ selectivities of Ni-supported catalysts varied in the order of Ni/MgO > Ni/ZnO > Ni/Al₂O₃ > Ni/ZrO. Although the type of support had a minimal effect on H₂ yield, a significant effect was observed on the decrease in CO yield. Basic oxide supports such as MgO and ZnO favored water–gas shift reactions, thus increasing H₂ yields. The acidic support such as Al₂O₃ did not enhance the water–gas shift reaction. Hence, Ni/Al₂O₃ showed nearly double the CO yield as compared to the Ni/ZnO and Ni/MgO catalysts.

Okolie et al. [54] performed the SCWG of soybean straw using different Ni-based catalysts, catalyst supports, and promoters. ZrO₂ and Al₂O₃ proved to be the most effective supports for Ni-based catalysts. Both 10%Ni-ZrO₂ and 10%Ni-Al₂O₃ demonstrated higher H₂ yields than other catalyst supports (e.g., CNT, SiO₂/Al₂O₃, SiO₂, and AC). Therefore, the authors further studied the effects of K, Na, and Ce promoters on Ni-based catalysts supported by ZrO₂ and Al₂O₃. The 10%Ni-1%Ce/ZrO₂ catalyst demonstrated the highest H₂ yield of 10.9 mmol/g, followed by 10%Ni-1%K/ZrO₂ and 10%Ni-1%Na/ZrO₂. The relative increment in H₂ yield and total gas yield without using any promoters was more substantial with the Ce and K promoters than with the Na promoter. However, the Na promoter showed the highest H₂ yield with the Al₂O₃ support compared to the K and Ce promoters. The 10%Ni-1%Na/Al₂O₃ catalyst demonstrated the highest H₂ yield (10.8 mmol/g) compared to 10%Ni-Ce/Al₂O₃ and 10%Ni-1%K/Al₂O₃. The 10%Ni-1%Ce/ZrO₂ catalyst demonstrated an improved H₂ yield and excellent catalytic performance. Further analysis revealed that the Ce promoter could store oxygen species and eliminate coke formation and sintering of the catalysts, resulting in its high performance.

Su et al. [60] investigated the effects of La₂O₃ in promoting the Ni-La₂O₃/θ-Al₂O₃ catalyst in the SCWG of food waste. La enhanced the water–gas shift reaction, resulting in a high H₂ yield. La also inhibited the methanation reaction, which is a major limitation of Ni-based catalysts. La also improved the metal dispersion, which increased the catalytic activity. Chowdhury et al. [61] also reported that Ni/Al₂O₃ with an La promoter can lead to excellent catalytic activity in the SCWG of food waste. Ni/9%La-Al₂O₃ showed high H₂ and gas yields. La improved the mesoporous structure and increased the dispersion of Ni, which enhanced the water–gas shift reaction and increased the H₂ yield. Ni/9%La-Al₂O₃ also demonstrated high stability, which could be attributed to its better anti-carbon deposition property.

Mastuli et al. [62] compared doped and supported Zn and Ni catalysts on MgO support in the SCWG of oil palm frond. The doped catalysts had high surface areas, high stability, and high-activity basic sites, resulting in high H₂ yields compared to supported catalysts. Zn-based catalysts showed higher H₂ yields than Ni-based catalysts for both supported and doped catalysts. Mastuli et al. [63] further investigated the structural and catalytic effects of Mg_{1-x}Ni_xO nanomaterial as a catalyst. They synthesized Mg_{1-x}Ni_xO nanomaterial via a self-propagating combustion method in the SCWG of oil palm frond. As the Ni content increased, the cell volume decreased linearly. This increased the specific surface area and improved the basic properties of the catalyst. The Mg_{0.8}Ni_{0.2}O catalyst with the highest Ni content demonstrated the highest gas and H₂ yields.

Li et al. [64] demonstrated that the formation of the char layer could be minimized using co-precipitated Ni-Mg-Al catalysts. They varied the Mg-Al molar ratio in the catalyst and investigated its effects in the SCWG of glucose. The catalysts favored H₂ production, resulting in high H₂ selectivity. Furthermore, Mg inhibited graphitic carbon formation because of its neutralizing action on alumina acidic sites, thus increasing the lifespan of the catalysts. However, the subsequent increase in Mg loading formed the MgNiO₂ complex, which limited the activity of Ni metal.

Li et al. [65] also studied the stability and activities of various wet-impregnated Mg-promoted Ni catalysts on Al₂O₃ and CNT supports in the SCWG of glycerol. The stability studies showed the loss of Al, which resulted in deactivation of the Mg-promoted

activity over repeated use. Additionally, SCWS-synthesized catalysts are also synthesized in an environmentally friendly way as they do not require any organic solvents or robust chemical compounds.

Li et al. [71] studied and proposed a catalytic mechanism in the SCWG of dewatered sewage sludge and various model compounds using AlCl_3 combined with Ni, KOH, or K_2CO_3 catalysts and oxidants (e.g., H_2O_2 , $\text{K}_2\text{S}_2\text{O}_8$, and CaO_2). AlCl_3 - H_2O_2 demonstrated the highest gas yields, followed by AlCl_3 - $\text{K}_2\text{S}_2\text{O}_8$. AlCl_3 combined with Ni, KOH, CaO, or K_2CO_3 catalysts resulted in low H_2 yields as compared to AlCl_3 alone. However, using $\text{K}_2\text{S}_2\text{O}_8$ or H_2O_2 alone decreased the H_2 yield. The H_2 yield decreased, and gasification efficiency increased with a rise in the addition of oxidants. Interestingly, AlCl_3 - H_2O_2 (8:2) showed the highest gas yield, followed by AlCl_3 - $\text{K}_2\text{S}_2\text{O}_8$ (8:2) and AlCl_3 . For the AlCl_3 -catalyzed SCWG of the model compound, glycerol resulted in the highest H_2 yield, followed by guaiacol, glucose, alanine, and humic acid. Al_2Cl_3 - H_2O_2 increased the H_2 yield of humic acid by 17% but decreased the H_2 yields of glucose and glycerol by 20% and 12%, respectively, compared to the AlCl_3 catalyst. The authors also proposed a catalytic mechanism in the SCWG of dewatered sewage sludge with an AlCl_3 - H_2O_2 catalyst. They proposed that AlCl_3 promoted the cleavage of the C–C bond with Al_3^+ ions. The Al_3^+ ions increased the acidity of SCW by reacting with water and forming $\text{Al}(\text{OH})_3$ and H^+ ions. $\text{Al}(\text{OH})_3$ further underwent dehydration to form $\text{AlO}(\text{OH})$, which formed precipitates in water. The H^+ and Cl^- ions enhanced the gasification of intermediate compounds to produce H_2 , thus increasing the H_2 yield. H_2O_2 further enhanced the gasification of benzene-containing monomers by favoring the steam reforming reaction. In the case of sewage sludge, H^+ generated via Al_3^+ deposition further enhanced the ring-opening activity of H_2O_2 to promote the decomposition of benzene-containing monomers into small molecules. These small organic molecules were further gasified by the combined catalytic effects of Cl^- and H^+ ions to increase H_2 yields.

Although Ni-based catalysts demonstrate improvement in gasification efficiency, they suffer from deactivation mainly because of tar formation and coke deposition [72]. Despite the high activity of Ni/ γ - Al_2O_3 -based catalysts, they still suffer from various issues, such as sintering, formation of Ni/ Al_2O_4 complexes, and transformation of the γ - Al_2O_3 phase to the α - Al_2O_3 phase. These issues significantly hamper the catalysts' stability. This is a severe issue for alumina-supported catalysts due to the ready conversion of intermediate products adsorbed on the acidic site into carbon, which deactivates Ni-based catalysts. The addition of alkali promoters can suppress cracking and polymerization reactions. Alkali promoters can also neutralize the acidic sites of alumina supports. Thus, alkali promoters can significantly reduce carbon formation.

3.1.2. Ruthenium-Based Catalysts

Ru-based catalysts with promising metal dispersion are more reactive at low temperatures than Ni-based catalysts [73]. Ru-based catalysts have higher surface areas and distribution than Ni-based catalysts. Therefore, high surface area and more metal distribution can be achieved with relatively low Ru metal loading on the support material. Nguyen et al. [74] also confirmed that Ru-based catalysts show higher catalytic activities per metallic mass than Ni-based catalysts. Additionally, Ru-based catalysts are highly resistant to oxidation and hydrothermal conditions compared to Ni-based catalysts. Ru-based catalysts have higher activities toward hydrogenation and C–C bond cleavage [75]. When compared to other expensive transition metals, Ru-based catalysts exhibit the highest activity and H_2 selectivity.

As opposed to Ni-based catalysts, Ru-based catalysts are more susceptible to deactivation by sulfur poisoning [76]. To overcome sulfur sintering, a sacrificial agent with a relatively high affinity towards sulfur can be used to protect Ru from sulfur sintering. Peng et al. [77] used ZnO as a sacrificial agent with Ru/C catalysts to study the SCWG of microalgae (*Chlorella vulgaris*). ZnO showed high mechanical stability and sulfur adoption performance, which minimized Ru metal sintering. Despite Ru-based catalysts having

high surface areas, high dispersion, and high catalytic performance, the relatively low cost of Ni-based catalysts makes them preferable for large-scale industrial applications over Ru-based catalysts.

Kang et al. [29] also observed that Ru/Al₂O₃ showed the highest metal dispersion compared to Ni-based catalysts. They concluded that 5%Ru/Al₂O₃ demonstrated a higher H₂ yield than the 5%Ni/Al₂O₃ catalyst in the SCWG of cellulose and lignin. Therefore, for the same metal loading, Ru-based catalysts had higher H₂ yields than Ni-based catalysts. Nanda et al. [55] compared Ru/Al₂O₃ with Ni/Si-Al₂O₃, K₂CO₃, and Na₂CO₃ catalysts in the SCWG of waste cooking oil. The order of H₂ yield was Ru/Al₂O₃ > Ni/Si-Al₂O₃ > K₂CO₃ > Na₂CO₃. The effects of metal loading showed that 5 wt% Ru/Al₂O₃ resulted in the maximum H₂ yield.

The superior catalytic performance of Ru/Al₂O₃ catalysts has also been reported in the SCWG of glucose and guaiacol [75,78]. In the SCWG of glucose, the Ru/Al₂O₃ catalyst inhibited the production of furfural and 5-hydroxymethylfurfural while favoring the degradation of intermediates such as phenols, ketones, acids, and arenes [75]. Enhanced gasification of intermediates improved process efficiency and increased total gas and H₂ yields while preventing the formation of char. During the SCWG of guaiacol, Ru/Al₂O₃ catalysts enhanced the conversion of phenol to cyclohexanol by favoring the hydrogenation reaction and the conversion of cyclohexanol to hexanone or hexenol by favoring ring-opening reactions [78]. Hexanone and hexenol can further decompose into small gaseous molecules, including H₂. Thus, Ru/Al₂O₃ improved H₂ and total gas yields while minimizing char and tar formation.

Zhang et al. [58] observed the effects of Ni and Ru bimetallic catalysts supported on γ -Al₂O₃. They recommended the use of Ni and Ru bimetallic catalysts supported on γ -Al₂O₃ in the SCWG of glucose to achieve high activity and H₂ selectivity. Hossain et al. [52] further investigated various bimetallic Ni-Ru/Al₂O₃-supported aerogel catalysts. Ni-Ru/Al₂O₃ aerogel catalysts demonstrated 1.3- and 1.6-times higher H₂ yields than mesoporous and wet-impregnated synthesized Ni-Ru/Al₂O₃ catalysts for the same amount of metal loading. The aerogel catalysts showed high and uniform metal particle dispersion with strong interaction between the support and active metal. The high catalytic performance of the aerogel catalysts was due to the supercritical CO₂ drying step during aerogel catalyst synthesis, which improved the surface area and reactant diffusivity. A significant decrease in coke formation was also observed with the aerogel catalysts due to their low acidity. This resulted in high stability and activities of the aerogel catalysts.

Tushar et al. [79] confirmed the catalytic effects of Ni and Ru catalysts. They investigated ten different combinations of Ni and Ru catalysts on various supports, such as γ -Al₂O₃ and ZrO₂. Overall, Ni-Ru/ γ -Al₂O₃-ZrO₂ demonstrated the maximum H₂ yields and high carbon gasification efficiency. Ni-Ru/ γ -Al₂O₃-ZrO₂ also demonstrated high stability and activities over repeated use. In another study, dual-component catalysts having equal amounts of Ru/C-Ru/C demonstrated better catalytic activities than single-component catalysts [80].

Yang et al. [81] investigated the kinetics and intermediate products of Ni-Ru/Al₂O₃ bimetallic catalysts for the SCWG of phenol. They proposed that phenol converted into an enol intermediate via a partial hydrogenation reaction. Furthermore, enol rapidly formed cyclohexanone. This observation was different from the mechanism proposed by Zhu et al. [78] where cyclohexanone was considered as an intermediate product for the formation of cyclohexanol. The kinetic study revealed that phenol was more difficult to gasify than the intermediate compounds. Interestingly, steam reforming of cyclohexanone was not the main contributor to H₂ production due to its lower concentration than phenol.

3.1.3. Other Heterogeneous Catalysts

Apart from Ni and Ru, other transition metals such as Pt, Co, and Rh (supported or unsupported) are also used as heterogeneous catalysts in the SCWG process. Karakuş et al. [49] investigated Pt/Al₂O₃ and Ru/Al₂O₃ catalysts in the SCWG of

2-propanol. Their results showed that the H₂ selectivity of Pt/Al₂O₃ was relatively higher than that of Ru/Al₂O₃ due to enhancement of the methanation reaction, which produced CH₄ at the expense of H₂. Pairojpiriyakul et al. [82] used Co-based catalysts on a variety of supports, such as α -Al₂O₃, ZrO₂, γ -Al₂O₃, La₂O₃, and yttria-stabilized zirconia (YSZ), in the SCWG of glycerol. The highest H₂ yield was obtained with Co/YSZ. In addition, increasing the Co loading up to 10% improved the gasification efficiency of glycerol and H₂ production. However, a further increase in the Co loading decreased both H₂ yield and glycerol conversion.

Deactivation, sintering, and poisoning of heterogeneous catalysts by sulfur or coke is still a major challenge. Additionally, heterogeneous catalysts oxidize the elemental sulfur and chlorine in biomass to acids. Retention of these acids in the liquid products of SCWG poses a serious challenge for its disposal and/or recycling. The non-polar nature of SCW dissolves the organic compounds during hydrothermal gasification but the inorganic components, including the active metal (catalyst) and mineral matter (catalyst support), can precipitate and form agglomerates in the reactor if not removed properly. The gradual deposition of these precipitates and agglomerates can corrode the reactor during high-temperature and high-pressure operations [83]. Nevertheless, more advancements are needed to address these challenges to synthesize suitable heterogeneous catalysts with high activity, regenerability, and stability, with resistance to sintering and deactivation.

3.2. Metal Oxide Catalysts

Metal oxide catalysts are rarely used in the SCWG process and very little literature is available on their catalytic performance in SCWG processes. They are generally used as supports to improve the stability and activities of metal-supported catalysts. The most common metal oxides used in SCWG processes are RuO₂, ZrO₂, and CeO₂. Cao et al. [84] compared different metal oxides catalysts such as V₂O₅, MnO₂, Cr₂O₃, Fe₂O₃, CuO, Co₂O₃, ZnO, MoO₃, ZrO₂, SnO₂, CeO₂, and WO₃ in SCWG of glucose. Among all metal oxide catalysts, Cr₂O₃, CuO, and WO₃ showed high gasification efficiencies compared to Fe₂O₃, ZnO, and ZrO₂. The H₂ yields decreased with almost all metal oxide catalysts, except Cr₂O₃, which improved the H₂ yield.

Various co-precipitated binary metal oxide catalysts, such as CeO₂-ZrO₂, CuO-ZnO, and Fe₂O₃-Cr₂O₃, have demonstrated high catalytic performance in SCWG [85,86]. Cao et al. [85] showed that in the SCWG of lignin, the CuO-ZnO catalyst demonstrated high catalytic performance with a high H₂ yield and better gasification efficiency, followed by Fe₂O₃-Cr₂O₃ and CeO₂-ZrO₂. However, in the SCWG of cellulose, Fe₂O₃-Cr₂O₃ showed a greater H₂ yield and high carbon gasification efficiency, followed by CuO-ZnO and CeO₂-ZrO₂. This was due to the higher oxygen content of cellulose compared to lignin. Thus, oxygen released by metal oxide catalysts had less pronounced effects in the SCWG of cellulose. Additionally, the H₂ yield from cellulose was less than that from lignin, which also decreased the reducibility of the reaction medium. The catalytic mechanism of binary metal oxide catalysts showed that CeO₂ was the main active component in the CeO₂-ZrO₂ catalyst [86]. CeO₂ distributed on ZrO₂ released active oxygen via redox reactions to enhance the SCWG process. ZrO₂ also absorbed active H₂ and small intermediates to increase contact between the intermediates and CeO₂ for improved catalytic performance. In CuO-ZnO, Cu was the main active component, which released oxygen species (Figure 5). ZnO acted as a structural stabilizer, promotor and absorbent for sulfur in the CuO-ZnO supported catalyst.

Onwudili [87] studied the detailed catalytic mechanism of RuO₂/ γ -Al₂O₃ in the SCWG of municipal solid waste. RuO₂/ γ -Al₂O₃ drastically increased H₂, CH₄, and CO₂ yields while significantly improving gasification efficiency. The high yield of H₂ was due to enhancement of the water-gas shift reaction by the catalytic action of RuO₂/ γ -Al₂O₃. In addition, the enhancement of methanation of CO or CO₂ and hydrogenolysis of C-C hydrocarbons resulted in a high CH₄ yield. Improvement in the yields of the reduction product (CH₄) and oxidation product (CO₂) indicated the involvement of the RuO₂/

γ -Al₂O₃ catalyst in Ru(IV) and Ru(0) cyclic redox reactions. Reduction of Ru(IV) into Ru(0) was essential for the SCWG process, whereas oxidation of Ru(0) into Ru(IV) was necessary for the catalytic process. The primary synergetic effects were due to the improvement of the dispersion of RuO₂ on γ -Al₂O₃, which resulted in enhanced carbon gasification efficiency.

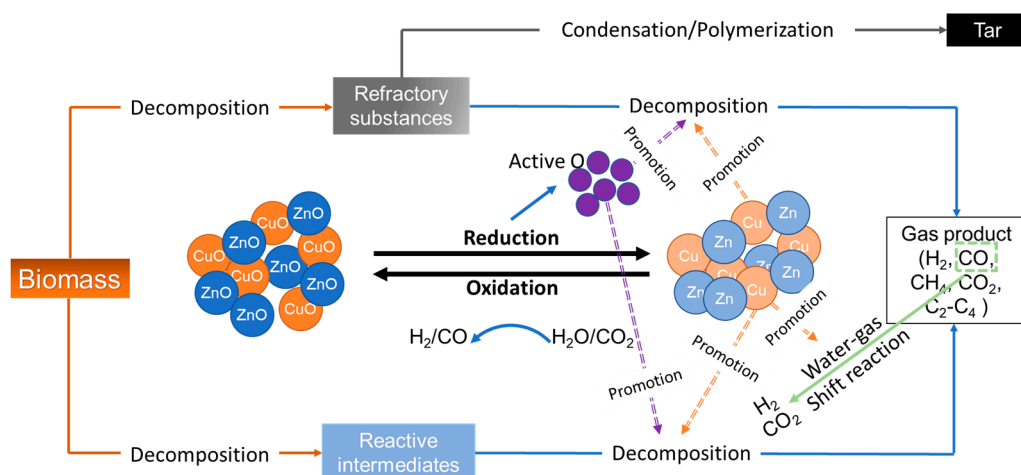


Figure 5. Catalytic mechanism of CuO-ZnO in SCWG of biomass (adapted with permission from Cao et al. [85]).

Samiee-Zafarghandi et al. [88] compared MnO₂/SiO₂ and NiO/SiO₂ catalysts in the SCWG of microalgae *Chlorella*. MnO₂/SiO₂ demonstrated the highest H₂ yield (1.1 mmol/g) compared to NiO/SiO₂ (0.6 mmol/g) and non-catalytic SCWG (0.2 mmol/g). Therefore, NiO/SiO₂ was less active than the supported MnO₂/SiO₂. Borges et al. [89] investigated the Ni/Fe₂O₄ catalyst in the SCWG of *Eucalyptus* wood chips. Ni/Fe₂O₄ enhanced the H₂ yield and decreased the char yield. Further investigation showed that Ni/Fe₂O₄ favored the water–gas shift and steam reforming reactions, thus increasing H₂ yield and decreasing CH₄ yield. It also demonstrated good stability and recyclability despite the coke deposit [90].

4. Novel Carbon-Based Catalysts Used in Hydrothermal Gasification

Carbon-based supports can also be used with transition metals in the SCWG of biomass. Their high surface areas along with the renewable and biodegradable nature of activated carbon and other carbon-based supports make them sustainable catalytic materials. Table 3 summarizes some notable studies on the use of carbon-based catalysts for SCWG processes [65,71,91–94]. Taylor et al. [95] compared Ni/AC and Ru/AC with other catalysts such as KOH, Trona, dolomite, and Borax in the SCWG of wood chips. Both Ni/AC and Ru/AC demonstrated higher H₂ yields because of improved water–gas shift compared to other non-carbonaceous catalysts.

Table 3. Notable studies on SCWG of waste biomass assisted by novel carbonaceous catalysts.

Feedstock	Catalyst	Operating Conditions	Main Findings	Reference
Almond shell	Hydrochar generated from SCWG of wheat straw and algae (<i>Cladophora glomerata</i>)	<ul style="list-style-type: none"> Temperature: 460 °C Reaction time: 10 min Feed-to-water ratio: 0.01 Pressure: 25 MPa Reactor: Batch 	<ul style="list-style-type: none"> Hydrochar from algal and wheat straw demonstrated H₂ yields of 11.6 and 10.8 mmol/g, respectively. Algal hydrochar showed higher H₂ yield, H₂ selectivity, and total gas yield due to the presence of alkali and alkaline earth metals, which enhanced the water–gas shift reaction. 	Safari et al. [91]

Table 3. Cont.

Feedstock	Catalyst	Operating Conditions	Main Findings	Reference
Banana pseudo-stem	In-situ impregnated biomass with Fe, Ru, and Ni	<ul style="list-style-type: none"> • Temperature: 600 °C • Reaction time: 1 h • Pressure: 22–25 MPa • Reactor: Batch 	<ul style="list-style-type: none"> • Impregnated metals dramatically improved gasification efficiency and H₂ yields. • Ni-impregnated biomass showed the highest H₂ yield (11.1 mmol/g) followed by Ru (8.8 mmol/g) and Fe (4.2 mmol/g). • Ni nanoparticles enhanced cracking and reforming reactions. • Ru nanoparticles favored the methanation reaction. • Fe nanoparticles formed an oxide layer and promoted H₂ yields. 	Kumar et al. [92]
Dewater sewage sludge and model compounds	AlCl ₃ with Ni, KOH, and K ₂ CO ₃ catalysts with H ₂ O ₂ , K ₂ S ₂ O ₈ , and CaO ₂ oxidants	<ul style="list-style-type: none"> • Temperature: 400 °C • Reaction time: 30 min • Feed concentration: 5 wt% • Pressure: 24 MPa • Reactor: Batch 	<ul style="list-style-type: none"> • AlCl₃-K₂CO₃ led to the highest H₂ yield (0.85 mmol/g) followed by Ni (0.8 mmol/g) and KOH (0.7 mmol/g), compared to using AlCl₃ alone (7.8 mmol/g). • Oxidants performed better than catalysts. • AlCl₃ combined with H₂O₂ showed the highest H₂ yield of 8.9 mmol/g. However, oxidants alone decreased the H₂ yield. • Glycerol demonstrated the highest H₂ yield followed by guaiacol, glucose, alanine, and humic acid with AlCl₃. 	Li et al. [71]
Glycerol	Ni/MgAl ₂ O ₄ -Al ₂ O ₃ , Ni/Al ₂ O ₃ , and Ni/CNT	<ul style="list-style-type: none"> • Temperature: 425 °C • Reaction time: 54 s • Feed concentration: 5 wt% • Pressure: 25.2 MPa • Reactor: Continuous 	<ul style="list-style-type: none"> • Ni/CNT demonstrated high stability with superior carbon gasification efficiency. • Ni/CNT improved the H₂ yield by 2.7 times compared to the non-catalytic SCWG. • Ni/MgAl₂O₄ showed the highest H₂ yield (1.5 mol/mol) followed by Ni/Al₂O₃ (1.0 mol/mol) and Ni/CNT (0.8 mol/mol). 	Li et al. [65]
Pinewood and wheat straw	In-situ Ni impregnation	<ul style="list-style-type: none"> • Temperature: 500 °C • Reaction time: 45 min • Pressure: 23–25 MPa • Reactor: Batch 	<ul style="list-style-type: none"> • In-situ Ni-impregnated pinewood showed improvements of 59%, 40%, and 34% in H₂ yield, total gas yield, and carbon gasification efficiency, respectively, compared to non-catalytic run. • Ni impregnation resulted in an H₂ yield of 5.8 mmol/g from wheat straw and 2.8 mmol/g with pinewood. • High H₂ yield with wheat straw was attributed to a better distribution of Ni nanoparticles in wheat straw. 	Nanda et al. [93]
Sugarcane bagasse	Ru/AC and Ru/TiO ₂	<ul style="list-style-type: none"> • Temperature: 400 °C • Reaction time: 15 min • Pressure: 22–25 MPa • Reactor: Batch 	<ul style="list-style-type: none"> • Ru/AC demonstrated superior activity compared to Ru/TiO₂ with near-complete gasification of sugarcane bagasse in 15 min compared to 30 min using Ru/TiO₂. • H₂ yield increased with repeated use of Ru/AC catalyst but it suffered from deactivation leading to a significant reduction in its activity. 	Osada et al. [94]

Yamaguchi et al. [96] investigated various metals (e.g., Ru, Ni, Pt, Rh and Pd) supported on activated carbon in the SCWG of woody biomass. The Ru/AC catalysts demonstrated the highest gas yields, followed by Rh/AC, Pt/AC, Pd/AC, and Ni/AC. Ru/AC showed the highest activity for lignin gasification. However, it showed an inferior H₂ yield, which was due to enhancement of the methanation reaction, which consumed H₂. Interestingly, the Pd/AC catalyst demonstrated the highest H₂ yield, followed by Ru/AC, Pt/AC, Rh/AC, and Ni/AC. Thus, Pd/AC showed the best H₂ yield but poor gas yields, whereas Ni/AC showed the lowest gas and H₂ yields. Activated carbon also improved the H₂ yield over a wide range of reaction temperatures.

Osada et al. [94] investigated TiO₂ and activated carbon as supports for Ru catalysts in the SCWG of lignin, cellulose, and sugarcane bagasse. Ru/AC demonstrated the highest gasification efficiency with near-complete gasification of sugarcane bagasse in 15 min. For the same amount of Ru metal, Ru/AC showed slightly higher activity as compared to Ru/TiO₂ catalysts. This was due to the high Ru metal dispersion of 51% in the Ru/AC catalyst as compared to 27% metal dispersion in Ru/TiO₂. However, the gas yield and composition of both catalysts were the same when 100% carbon conversion was achieved. This indicated that the equilibrium gas yield and composition did not have any correlation with metal dispersion. For the Ru/AC catalysts, repetitive use increased H₂ selectivity but decreased CH₄ selectivity due to disintegration of the active sites for the methanation reaction. However, Ru/AC suffered from deactivation since its activity decreased significantly after repetitive use. Therefore, more active and durable AC-based catalysts need to be developed to overcome these challenges. Yamaguchi et al. [96] reported that Ru/ γ -Al₂O₃ demonstrated high gasification activity but low stability as the crystallographic phase of γ -Al₂O₃ transformed into α -Al₂O₃.

CNT is another carbon-based support that has a large surface area, high heat conductivity, excellent chemical and physical stability, and a tunable porous structure. Among SCWS-prepared metal-impregnated carbon catalysts, CNT-based catalysts showed higher activities and stability than active carbon and Al₂O₃ supported catalysts [97]. At reaction conditions of 480 °C, 25 MPa, and 10–50 h, Ni/CNT resulted in the highest H₂, CO, CH₄, and total gas yields, followed by Ni/AC, Ni/Al₂O₃, and Ni catalysts. Ni/CNT maintained its high activity even at a longer reaction time of 50 h, whereas Ni/AC and Ni/Al₂O₃ significantly dropped their activities after 30 h of use. This was primarily due to the leaching of active Ni metal in the Ni/AC and Ni/Al₂O₃ catalysts.

Rashidi and Tavasoli [98] evaluated the effects of a copper promoter on Ni/CNT catalysts in the SCWG of sugarcane bagasse. Cu-promoted Ni/CNT was found to increase the H₂ and total gas yields but decreased the CH₄ yield. Thus, Cu-promoted Ni/CNT catalysts overcome the methanation tendency of Ni, which is a major limiting factor of Ni-based catalysts. Azadi et al. [28] reported that Ni-Cu/CNT showed a nearly ten-fold increase in H₂ yield and 40 times less CH₄ yield with a significant reduction in CO₂ yield. Thus, Cu-promoted Ni/CNT catalysts have high H₂ selectivity and low CH₄ and CO₂ selectivities. Li et al. [65] confirmed the high catalytic stability over repeated use of Ni/CNT catalysts in the SCWG of glycerol. de Vlieger et al. [99] also showed the high stability of Pd/CNT catalysts in the SCWG of ethylene glycerol. Pt/CNT exhibited no mass loss with no change in the size and distribution of Pt particles on CNT during SCWG.

Carbonaceous materials such as hydrochar and biochar are also potential materials for the development of catalysts. Safari et al. [91] investigated the performance of catalysts developed from the hydrochars of green algae (*Cladophora glomerata*) and wheat straw in the SCWG of almond shells. The high amounts of alkali and alkaline earth metals in the hydrochar samples enhanced the cracking of biopolymers and favored the water–gas shift reaction, thus increasing the H₂ yield. The total gas yield and H₂ fraction were selectively improved from 26.7 mmol/g and 41% in the non-catalytic run to 29.2 mmol/g and 58%, respectively, when wheat straw hydrochar was used as the catalyst. The total gas yield and H₂ concentration also increased to 31.1 mmol/g and 60%, respectively, when green algae hydrochar was used as the catalyst in the SCWG of almond shells.

Another novel method for catalytic SCWG is the in-situ impregnation of metal nanoparticles in biomass feedstock. This approach can overcome the issue of deactivation encountered by conventional catalysts and help to reduce the cost of catalyst preparation. Nanda et al. [93] carried out the SCWG of pinewood and wheat straw impregnated with Ni-nanoparticles. Ni-impregnated biomasses demonstrated high H₂, CO₂, and CH₄ yields compared to the raw feedstocks. Huang et al. [100] also used in-situ-generated Ni particles using nickel acetate as a precursor for the gasification of glucose in SCW. In-situ-generated Ni catalysts demonstrated superior catalytic performance compared to nickel wire catalysts. They also proved the role of in-situ generated Ni particles from nickel acetate in enabling the catalytic production of H₂ during SCWG of glucose.

Kumar and Reddy [101] investigated the SCWG of in-situ Ni-impregnated sugarcane bagasse and lemon peels and compared the results with the Raney nickel catalyst. They used nickel nitrate hexahydrate salt as a precursor for the in-situ generation of nickel nanoparticles. Both Ni-impregnated biomasses demonstrated significantly higher gas yields, H₂ yields, and carbon gasification efficiencies than Raney nickel. Ni-impregnated sugarcane bagasse achieved higher carbon gasification efficiency, gas yield, and H₂ yield than Ni-lemon peel. Kumar and Reddy [92] also performed the SCWG of banana pseudostem using impregnation of Ni, Ru, and Fe metals onto the biomass as the support material. The H₂ yields and gasification efficiencies of the metals were in order of Ni > Ru > Fe. The superior performance of Ni to act as an in-situ nanocatalyst is due to its ability to effectively cleave C–H and C–C bonds for improved reforming reactions [102]. However, very little literature is available on the development of in-situ nanocatalysts impregnated onto biomass for proper assessment of their robustness, stability, regeneration, and post-gasification compared to commercially available homogeneous and heterogeneous catalysts. One of the limitations in the design of such novel catalysts can be the presence of lignin and other mineral matter in the biomass [103,104], which can hinder the penetration of catalytic nanoparticles within the cell wall. Therefore, more research is needed for a better understanding of such catalysts and to address these limitations.

5. Conclusions and Perspectives

SCWG is a promising technology for the sustainable production of H₂ due to its various advantages over other thermochemical processes. SCWG has shown its potential for converting a wide variety of low-value biomasses into high-value H₂-rich gas products. This can serve as a green alternative to the steam methane reforming process due to the renewable and clean nature of biomass sources compared to fossil fuels. However, SCWG requires high energy input to achieve supercritical conditions. Nonetheless, catalysts are used to achieve high gas yields and process efficiencies even at near-critical conditions.

Various homogeneous and heterogeneous catalysts have been studied to achieve high H₂ yields at low temperatures in SCWG processes. Although homogeneous catalysts are suitable compared to heterogeneous catalysts, they suffer from recovery issues. This also increases the cost of the process and hinders its use in large-scale industrial applications. On the other hand, heterogeneous catalysts are relatively easier to recover, but they can suffer from deactivation. Deactivation of heterogeneous catalysts can occur for various reasons, such as fouling, poisoning, sintering, and char formation. Transition metal catalysts (e.g., Ni, Cu, Co, and Ru) have demonstrated excellent performance in enhancing SCWG reactions. Ru- and Ni-based catalysts are the most widely used catalysts owing to their superior performance in SCWG processes, especially in water–gas shift, hydrogenation, and methanation reactions. Novel catalysts such as activated carbon, char, CNT, and lignocellulosic biomass impregnated with catalytic nanoparticles have demonstrated promising potential to achieve comparable catalytic performance and renewability in SCWG reactions.

It cannot be denied that SCWG is an innovative and viable technology for producing combustible gases with higher selectivity to individual gas components using catalysts. However, a detailed study of the economic viability and technical feasibility of these catalysts is needed. New developments in the field of catalysts can facilitate the commer-

cialization of SCWG technology. Extensive research strategies are required to tackle the unique challenges faced by SCWG technology that prevents its scalability and commercialization. Some of the common challenges are associated with reactor corrosion, plugging due to salt and mineral precipitation, the requirement of special reactor set-up resistant to high temperatures, high pressures, and corrosion, coking of catalyst supports, as well as catalyst poisoning, sintering, and deactivation. The techno-economic, environmental, and lifecycle viability of SCWG technology on a commercial scale is also contingent on the efficient conversion of feedstocks, catalyst recovery, regeneration and reuse, effective separation of gas, liquid, and solid products, as well as upgrading and applications of main products and co-products. Nonetheless, SCWG remains an appealing technology with many benefits in the use of water as a source of aqueous reaction media to valorize complex feedstocks and pollutants under environmentally benign conditions while addressing the issues of waste management and clean energy recovery.

Author Contributions: Conceptualization, K.K., P.B. and S.N.; validation, K.K., P.B. and S.N.; investigation, K.K., P.B. and S.N.; resources, A.K.D.; data curation, K.K., P.B. and S.N.; writing—original draft preparation, K.K., P.B. and S.N.; writing—review and editing, K.K., P.B., S.N. and A.K.D.; visualization, K.K., P.B. and S.N.; supervision, A.K.D.; project administration, A.K.D.; funding acquisition, A.K.D. All authors have read and agreed to the published version of the manuscript.

Funding: The authors would like to thank the Natural Sciences and Engineering Research Council of Canada (NSERC) and the Canada Research Chairs (CRC) program for funding this work.

Institutional Review Board Statement: Not applicable.

Informed Consent Statement: Not applicable.

Data Availability Statement: Not applicable.

Conflicts of Interest: The authors declare no conflict of interest.

References

1. Nanda, S.; Reddy, S.N.; Mitra, S.K.; Kozinski, J.A. The progressive routes for carbon capture and sequestration. *Energy Sci. Eng.* **2016**, *4*, 99–122. [CrossRef]
2. Our World in Data. CO₂ Emissions by Fuel or Industry, World. Available online: <https://ourworldindata.org/grapher/co2-emissions-by-fuel-line?facet=none> (accessed on 11 May 2023).
3. Jha, S.; Nanda, S.; Acharya, B.; Dalai, A.K. A review of thermochemical conversion of waste biomass to biofuels. *Energies* **2022**, *15*, 6352. [CrossRef]
4. Okolie, J.A.; Nanda, S.; Dalai, A.K.; Kozinski, J.A. Chemistry and specialty industrial applications of lignocellulosic biomass. *Waste Biomass Valor.* **2021**, *12*, 2145–2169. [CrossRef]
5. Okolie, J.A.; Patra, B.R.; Mukherjee, A.; Nanda, S.; Dalai, A.K.; Kozinski, J.A. Futuristic applications of hydrogen in energy, biorefining, aerospace, pharmaceuticals and metallurgy. *Int. J. Hydrogen Energy* **2021**, *46*, 8885–8905. [CrossRef]
6. Fan, L.; Tu, Z.; Chan, S.H. Recent development of hydrogen and fuel cell technologies: A review. *Energy Rep.* **2021**, *7*, 8421–8446. [CrossRef]
7. Nanda, S.; Rana, R.; Zheng, Y.; Kozinski, J.A.; Dalai, A.K. Insights on pathways for hydrogen generation from ethanol. *Sustain. Energy Fuels* **2017**, *1*, 1232–1245. [CrossRef]
8. Zang, G.; Sun, P.; Elgowainy, A.; Wang, M. Technoeconomic and life cycle analysis of synthetic methanol production from hydrogen and industrial byproduct CO₂. *Environ. Sci. Technol.* **2021**, *55*, 5248–5257. [CrossRef]
9. Kim, S.; Kwon, E.E.; Kim, Y.T.; Jung, S.; Kim, H.J.; Hubere, G.W.; Lee, J. Recent advances in hydrodeoxygenation of biomass-derived oxygenates over heterogeneous catalysts. *Green Chem.* **2019**, *21*, 3715–3743. [CrossRef]
10. Bello, S.S.; Wang, C.; Zhang, M.; Gao, H.; Han, Z.; Shi, L.; Su, F.; Xu, G. A review on the reaction mechanism of hydrodesulfurization and hydrodenitrogenation in heavy oil upgrading. *Energy Fuels* **2021**, *35*, 10998–11016. [CrossRef]
11. Nguyen, T.H.; Nguyen, Q.A.; Cao, A.N.T.; Ernest, T.; Nguyen, T.B.; Pham, P.H.T.; Nguyen, T.M. Hydrodemetallization of heavy oil: Recent progress, challenge, and future prospects. *J. Petrol. Sci. Eng.* **2022**, *216*, 110762. [CrossRef]
12. National Grid. The Hydrogen Colour Spectrum. Available online: <https://www.nationalgrid.com/stories/energy-explained/hydrogen-colour-spectrum> (accessed on 11 May 2023).
13. Finke, C.E.; Leandri, H.F.; Karumb, E.T.; Zheng, D.; Hoffmann, M.R.; Fromer, N.A. Economically advantageous pathways for reducing greenhouse gas emissions from industrial hydrogen under common, current economic conditions. *Energy Environ. Sci.* **2021**, *14*, 1517–1529. [CrossRef]

14. Rapiere, R. Estimating the Carbon Footprint of Hydrogen Production. *Forbes*. Available online: <https://www.forbes.com/sites/rapiere/2020/06/06/estimating-the-carbon-footprint-of-hydrogen-production/?sh=5cfba0b424bd> (accessed on 11 May 2023).
15. Sarangi, P.K.; Nanda, S. Biohydrogen production through dark fermentation. *Chem. Eng. Technol.* **2020**, *43*, 601–612. [[CrossRef](#)]
16. Reddy, S.N.; Nanda, S.; Dalai, A.K.; Kozinski, J.A. Supercritical water gasification of biomass for hydrogen production. *Int. J. Hydrogen Energy* **2014**, *39*, 6912–6926. [[CrossRef](#)]
17. Okolie, J.A.; Nanda, S.; Dalai, A.K.; Berruti, F.; Kozinski, J.A. A review on subcritical and supercritical water gasification of biogenic, polymeric and petroleum wastes to hydrogen-rich synthesis gas. *Renew. Sustain. Energy Rev.* **2020**, *119*, 109546. [[CrossRef](#)]
18. Okolie, J.A.; Rana, R.; Nanda, S.; Dalai, A.K.; Kozinski, J.A. Supercritical water gasification of biomass: A state-of-the-art review of process parameters, reaction mechanisms and catalysis. *Sustain. Energy Fuels* **2019**, *3*, 578–598. [[CrossRef](#)]
19. Schienbein, P.; Marx, D. Assessing the properties of supercritical water in terms of structural dynamics and electronic polarization effects. *Phys. Chem. Chem. Phys.* **2020**, *22*, 10462–10479. [[CrossRef](#)]
20. Correa, C.R.; Kruse, A. Supercritical water gasification of biomass for hydrogen production—Review. *J. Supercrit. Fluids* **2018**, *133*, 573–590. [[CrossRef](#)]
21. Masoumi, S.; Borugadda, V.B.; Nanda, S.; Dalai, A.K. Hydrochar: A review on its production technologies and applications. *Catalysts* **2021**, *11*, 939. [[CrossRef](#)]
22. Nanda, S.; Dalai, A.K.; Berruti, F.; Kozinski, J.A. Biochar as an exceptional bioresource for energy, agronomy, carbon sequestration, activated carbon and specialty materials. *Waste Biomass Valor.* **2016**, *7*, 201–235. [[CrossRef](#)]
23. Patra, B.R.; Mukherjee, A.; Nanda, S.; Dalai, A.K. Biochar production, activation and adsorptive applications: A review. *Environ. Chem. Lett.* **2021**, *19*, 2237–2259. [[CrossRef](#)]
24. Kang, K.; Nanda, S.; Hu, Y. Current trends in biochar application for catalytic conversion of biomass to biofuels. *Catal. Today* **2022**, *404*, 3–18. [[CrossRef](#)]
25. Khorasani, R.; Khodaparasti, M.S.; Tavakoli, O. Hydrogen production from dairy wastewater using catalytic supercritical water gasification: Mechanism and reaction pathway. *Int. J. Hydrogen Energy* **2021**, *46*, 22368–22384. [[CrossRef](#)]
26. Ghavami, N.; Özdenkçi, K.; Salierno, G.; Björklund-Sänkiäho, M.; De Blasio, C. Analysis of operational issues in hydrothermal liquefaction and supercritical water gasification processes: A review. *Biomass Convers. Bioref.* **2021**. [[CrossRef](#)]
27. Azadi, P.; Afif, E.; Azadi, F.; Farnood, R. Screening of nickel catalysts for selective hydrogen production using supercritical water gasification of glucose. *Green Chem.* **2012**, *14*, 1766–1777. [[CrossRef](#)]
28. Azadi, P.; Afif, E.; Foroughi, H.; Dai, T.; Azadi, F.; Farnood, R. Catalytic reforming of activated sludge model compounds in supercritical water using nickel and ruthenium catalysts. *Appl. Catal. B Environ.* **2013**, *134–135*, 265–273. [[CrossRef](#)]
29. Kang, K.; Azargohar, R.; Dalai, A.K.; Wang, H. Hydrogen production from lignin, cellulose and waste biomass via supercritical water gasification: Catalyst activity and process optimization study. *Energy Convers. Manag.* **2016**, *117*, 528–537. [[CrossRef](#)]
30. Madenoğlu, T.G.; Sağlam, M.; Yüksel, M.; Ballice, L. Hydrothermal gasification of biomass model compounds (cellulose and lignin alkali) and model mixtures. *J. Supercrit. Fluids* **2016**, *115*, 79–85. [[CrossRef](#)]
31. García-Jarana, M.B.; Portela, J.R.; Sánchez-Oneto, J.; de la Ossa, E.J.M.; Al-Duri, B. Analysis of the supercritical water gasification of cellulose in a continuous system using short residence times. *Appl. Sci.* **2020**, *10*, 5185. [[CrossRef](#)]
32. Sinağ, A.; Kruse, A.; Rathert, J. Influence of the heating rate and the type of catalyst on the formation of key intermediates and on the generation of gases during hydrolysis of glucose in supercritical water in a batch reactor. *Ind. Eng. Chem. Res.* **2004**, *43*, 502–508. [[CrossRef](#)]
33. Rönnlund, I.; Myréen, L.; Lundqvist, K.; Ahlbeck, J.; Westerlund, T. Waste to energy by industrially integrated supercritical water gasification—Effects of alkali salts in residual by-products from the pulp and paper industry. *Energy* **2011**, *36*, 2151–2163. [[CrossRef](#)]
34. Feng, H.; Zhou, Z.; Hantoko, D.; Zhong, L.; Rahim, D.A.; Fang, W.; Yan, M. Effect of alkali additives on desulfurization of syngas during supercritical water gasification of sewage sludge. *Waste Manag.* **2021**, *131*, 394–402. [[CrossRef](#)] [[PubMed](#)]
35. Nanda, S.; Dalai, A.K.; Kozinski, J.A. Supercritical water gasification of timothy grass as an energy crop in the presence of alkali carbonate and hydroxide catalysts. *Biomass Bioenergy* **2016**, *95*, 378–387. [[CrossRef](#)]
36. Kruse, A.; Bernolle, P.; Dahmen, N.; Dinjus, E.; Maniam, P. Hydrothermal gasification of biomass: Consecutive reactions to long-living intermediates. *Energy Environ. Sci.* **2010**, *3*, 136–143. [[CrossRef](#)]
37. Su, W.; Zhao, M.; Xing, Y.; Ma, H.; Liu, P.; Li, X.; Zhang, H.; Wu, Y.; Xia, C. Supercritical water gasification of hyperaccumulators for hydrogen production and heavy metal immobilization with alkali metal catalysts. *Environ. Res.* **2022**, *214*, 114093. [[CrossRef](#)]
38. Watanabe, M.; Sue, K.; Adschiri, T.; Inomata, H.; Smith, R.L.; Arai, K. Control of methanol oxidation by ionic behavior in supercritical water. *Chem. Commun.* **2001**, *1*, 2270–2271. [[CrossRef](#)] [[PubMed](#)]
39. Ge, Z.; Jin, H.; Guo, L. Hydrogen production by catalytic gasification of coal in supercritical water with alkaline catalysts: Explore the way to complete gasification of coal. *Int. J. Hydrogen Energy* **2014**, *39*, 19583–19592. [[CrossRef](#)]
40. Sinağ, A.; Kruse, A.; Maniam, P. Hydrothermal conversion of biomass and different model compounds. *J. Supercrit. Fluids* **2012**, *71*, 80–85. [[CrossRef](#)]
41. Nanda, S.; Reddy, S.N.; Hunter, H.N.; Dalai, A.K.; Kozinski, J.A. Supercritical water gasification of fructose as a model compound for waste fruits and vegetables. *J. Supercrit. Fluids* **2015**, *104*, 112–121. [[CrossRef](#)]

42. Yanik, J.; Ebale, S.; Kruse, A.; Saglam, M.; Yüksel, M. Biomass gasification in supercritical water: II. Effect of catalyst. *Int. J. Hydrogen Energy* **2008**, *33*, 4520–4526. [[CrossRef](#)]
43. Ferreira-Pinto, L.; Feirhrmann, A.C.; Corazza, M.L.; Fernandes-Machado, N.R.C.; dos Reis Coimbra, J.S.; Saldaña, M.D.A.; Cardozo-Filho, L. Hydrogen production and TOC reduction from gasification of lactose by supercritical water. *Int. J. Hydrogen Energy* **2015**, *40*, 12162–12168. [[CrossRef](#)]
44. Zhong, J.; Zhu, W.; Wang, C.; Mu, B.; Lin, N.; Chen, S.; Li, Z. Transformation mechanism of polycyclic aromatic hydrocarbons and hydrogen production during the gasification of coking sludge in supercritical water. *Chemosphere* **2022**, *300*, 134467. [[CrossRef](#)]
45. Leite, M.J.L.; Marques, I.R.; Proner, M.C.; Araújo, P.H.H.; Ambrosi, A.; Luccio, M.D. Catalytically active membranes for esterification: A review. *Chin. J. Chem. Eng.* **2023**, *53*, 142–154. [[CrossRef](#)]
46. Dreimann, J.; Lutze, P.; Zagajewski, M.; Behr, A.; Górak, A.; Vorholt, A.J. Highly integrated reactor–separator systems for the recycling of homogeneous catalysts. *Chem. Eng. Process. Process Intens.* **2016**, *99*, 124–131. [[CrossRef](#)]
47. Fadhel, A.J.; Pollet, P.; Liotta, C.L.; Eckert, C.A. Combining the benefits of homogeneous and heterogeneous catalysis with tunable solvents and nearcritical water. *Molecules* **2010**, *15*, 8400–8424. [[CrossRef](#)]
48. Zaera, F. Designing sites in heterogeneous catalysis: Are we reaching selectivities competitive with those of homogeneous catalysts? *Chem. Rev.* **2022**, *122*, 8594–8757. [[CrossRef](#)]
49. Karakuş, Y.; Aynacı, F.; Kıpçak, E.; Akgün, M. Hydrogen production from 2-propanol over Pt/Al₂O₃ and Ru/Al₂O₃ catalysts in supercritical water. *Int. J. Hydrogen Energy* **2013**, *38*, 7298–7306. [[CrossRef](#)]
50. Lu, Y.; Zhu, Y.; Li, S.; Zhang, X.; Guo, L. Behavior of nickel catalysts in supercritical water gasification of glucose: Influence of support. *Biomass Bioenergy* **2014**, *67*, 125–136. [[CrossRef](#)]
51. Lu, Y.; Jin, H.; Zhang, R. Evaluation of stability and catalytic activity of Ni catalysts for hydrogen production by biomass gasification in supercritical water. *Carbon Resour. Convers.* **2019**, *2*, 95–101. [[CrossRef](#)]
52. Hossain, M.Z.; Chowdhury, M.B.I.; Jhwar, A.K.; Charpentier, P.A. Supercritical water gasification of glucose using bimetallic aerogel Ru-Ni-Al₂O₃ catalyst for H₂ production. *Biomass Bioenergy* **2017**, *107*, 39–51. [[CrossRef](#)]
53. Onwudili, J.A.; Williams, P.T. Catalytic Supercritical Water Gasification of Plastics with Supported RuO₂: A Potential Solution to Hydrocarbons–Water Pollution Problem. *Process Saf. Environ. Prot.* **2016**, *102*, 140–149. [[CrossRef](#)]
54. Okolie, J.A.; Mukherjee, A.; Nanda, S.; Dalai, A.K.; Kozinski, J.A. Catalytic supercritical water gasification of soybean straw: Effects of catalyst supports and promoters. *Ind. Eng. Chem. Res.* **2021**, *60*, 5770–5782. [[CrossRef](#)]
55. Nanda, S.; Rana, R.; Hunter, H.N.; Fang, Z.; Dalai, A.K.; Kozinski, J.A. Hydrothermal catalytic processing of waste cooking oil for hydrogen-rich syngas production. *Chem. Eng. Sci.* **2019**, *195*, 935–945. [[CrossRef](#)]
56. Shen, L.; Xu, J.; Zhu, M.; Han, Y.F. Essential role of the support for nickel-based CO₂ methanation catalysts. *ACS Catal.* **2020**, *10*, 14581–14591. [[CrossRef](#)]
57. Furusawa, T.; Sato, T.; Saito, M.; Ishiyama, Y.; Sato, M.; Itoh, N.; Suzuki, N. The evaluation of the stability of Ni/MgO catalysts for the gasification of lignin in supercritical water. *Appl. Catal. A Gen.* **2007**, *327*, 300–310. [[CrossRef](#)]
58. Zhang, L.; Champagne, P.; Xu, C.C. Screening of supported transition metal catalysts for hydrogen production from glucose via catalytic supercritical water gasification. *Int. J. Hydrogen Energy* **2011**, *36*, 9591–9601. [[CrossRef](#)]
59. Adamu, S.; Razzak, S.A.; Hossain, M.M. Fluidizable Ni/Ce-Meso-Al₂O₃ for gasification of glucose: Effect of catalyst reduction on hydrogen selectivity. *J. Ind. Eng. Chem.* **2018**, *64*, 467–477. [[CrossRef](#)]
60. Su, H.; Kanchanapip, E.; Wang, D.; Zhang, H.; Antoni; Mubeen, I.; Huang, Z.; Yan, M. Catalytic gasification of food waste in supercritical water over La promoted Ni/Al₂O₃ catalysts for enhancing H₂ production. *Int. J. Hydrogen Energy* **2020**, *45*, 553–564. [[CrossRef](#)]
61. Chowdhury, M.B.I.; Hossain, M.Z.; Mazumder, J.; Jhwar, A.K.; Charpentier, P.A. La-based catalysts to enhance hydrogen production during supercritical water gasification of glucose. *Fuel* **2018**, *217*, 166–174. [[CrossRef](#)]
62. Mastuli, M.S.; Kamarulzaman, N.; Kasim, M.F.; Zainal, Z.; Matsumura, Y.; Taufiq-Yap, Y.H. Comparative study between supported and doped MgO catalysts in supercritical water gasification for hydrogen production. *Int. J. Hydrogen Energy* **2019**, *44*, 3690–3701. [[CrossRef](#)]
63. Mastuli, M.S.; Kasim, M.F.; Mahat, A.M.; Asikin-Mijan, N.; Sivasangar, S.; Taufiq-Yap, Y.H. Structural and catalytic studies of Mg_{1-x}Ni_xO nanomaterials for gasification of biomass in supercritical water for H₂-rich syngas production. *Int. J. Hydrogen Energy* **2020**, *45*, 33218–33234. [[CrossRef](#)]
64. Li, S.; Guo, L.; Zhu, C.; Lu, Y. Co-precipitated Ni–Mg–Al catalysts for hydrogen production by supercritical water gasification of glucose. *Int. J. Hydrogen Energy* **2013**, *38*, 9688–9700. [[CrossRef](#)]
65. Li, S.; Savage, P.E.; Guo, L. Stability and activity maintenance of Al₂O₃- and carbon nanotube-supported Ni catalysts during continuous gasification of glycerol in supercritical water. *J. Supercrit. Fluids* **2018**, *135*, 188–197. [[CrossRef](#)]
66. Li, S.; Guo, L. Stability and activity of a co-precipitated Mg promoted Ni/Al₂O₃ catalyst for supercritical water gasification of biomass. *Int. J. Hydrogen Energy* **2019**, *44*, 15842–15852. [[CrossRef](#)]
67. Kang, K.; Azargohar, R.; Dalai, A.K.; Wang, H. Hydrogen generation via supercritical water gasification of lignin using Ni-Co/Mg-Al catalysts. *Int. J. Energy Res.* **2017**, *41*, 1835–1846. [[CrossRef](#)]
68. Norouzi, O.; Safari, F.; Jafarian, S.; Tavasoli, A.; Karimi, A. Hydrothermal gasification performance of *Enteromorpha intestinalis* as an algal biomass for hydrogen-rich gas production using Ru promoted Fe–Ni/γ-Al₂O₃ nanocatalysts. *Energy Convers. Manag.* **2017**, *141*, 63–71. [[CrossRef](#)]

69. Zhu, B.; Li, S.; Wang, W.; Zhang, H. Supercritical water synthesized Ni/ZrO₂ catalyst for hydrogen production from supercritical water gasification of glycerol. *Int. J. Hydrogen Energy* **2019**, *44*, 30917–30926. [[CrossRef](#)]
70. Li, S.; Zhu, B.; Wang, W.; Zhang, H.; Li, Q. Efficient and stable supercritical-water-synthesized Ni-based catalysts for supercritical water gasification. *J. Supercrit. Fluids* **2020**, *160*, 104790. [[CrossRef](#)]
71. Li, Z.; Gong, M.; Wang, M.; Feng, A.; Wang, L.; Ma, P.; Yuan, S. Influence of AlCl₃ and oxidant catalysts on hydrogen production from the supercritical water gasification of dewatered sewage sludge and model compounds. *Int. J. Hydrogen Energy* **2021**, *46*, 31262–31274. [[CrossRef](#)]
72. Pattnaik, F.; Patra, B.R.; Okolie, J.A.; Nanda, S.; Dalai, A.K.; Naik, S. A review of thermocatalytic conversion of biogenic wastes into crude biofuels and biochemical precursors. *Fuel* **2022**, *320*, 123857. [[CrossRef](#)]
73. Al-Doghachi, F.A.J.; Islam, A.; Zainal, Z.; Saiman, M.I.; Embong, Z.; Taufiq-Yap, Y.H. High coke-resistance Pt/Mg_{1-x}Ni_xO catalyst for dry reforming of methane. *PLoS ONE* **2016**, *11*, e0146862. [[CrossRef](#)]
74. Nguyen, H.T.; Yoda, E.; Komiyama, M. Catalytic supercritical water gasification of proteinaceous biomass: Catalyst performances in gasification of ethanol fermentation stillage with batch and flow reactors. *Chem. Eng. Sci.* **2014**, *109*, 197–203. [[CrossRef](#)]
75. Zhu, C.; Guo, L.; Jin, H.; Huang, J.; Li, S.; Lian, X. Effects of reaction time and catalyst on gasification of glucose in supercritical water: Detailed reaction pathway and mechanisms. *Int. J. Hydrogen Energy* **2016**, *41*, 6630–6639. [[CrossRef](#)]
76. Hunston, C.; Baudouin, D.; Tarik, M.; Kröcher, O.; Vogel, F. Investigating active phase loss from supported ruthenium catalysts during supercritical water gasification. *Catal. Sci. Technol.* **2021**, *11*, 7431–7444. [[CrossRef](#)] [[PubMed](#)]
77. Peng, G.; Ludwig, C.; Vogel, F. Catalytic supercritical water gasification: Interaction of sulfur with ZnO and the ruthenium catalyst. *Appl. Catal. B Environ.* **2017**, *202*, 262–268. [[CrossRef](#)]
78. Zhu, C.; Guo, L.; Jin, H.; Ou, Z.; Wei, W.; Huang, J. Gasification of guaiacol in supercritical water: Detailed reaction pathway and mechanisms. *Int. J. Hydrogen Energy* **2018**, *43*, 14078–14086. [[CrossRef](#)]
79. Tushar, M.S.H.K.; Dutta, A.; Xu, C.C. Catalytic supercritical gasification of biocrude from hydrothermal liquefaction of cattle manure. *Appl. Catal. B Environ.* **2016**, *189*, 119–132. [[CrossRef](#)]
80. Duan, P.G.; Yang, S.K.; Xu, Y.P.; Wang, F.; Zhao, D.; Weng, Y.J.; Shi, X.L. Integration of hydrothermal liquefaction and supercritical water gasification for improvement of energy recovery from algal biomass. *Energy* **2018**, *155*, 734–745. [[CrossRef](#)]
81. Yang, M.; Zhang, J.; Guo, Y. Supercritical water gasification of phenol over Ni-Ru bimetallic catalyst: Intermediates and kinetics. *J. Supercrit. Fluids* **2020**, *160*, 104810. [[CrossRef](#)]
82. Pairojpiriyakul, T.; Croiset, E.; Kiatkittipong, W.; Kiatkittipong, K.; Arpornwichanop, A.; Assabumrungrat, S. Hydrogen production from catalytic supercritical water reforming of glycerol with cobalt-based catalysts. *Int. J. Hydrogen Energy* **2013**, *38*, 4368–4379. [[CrossRef](#)]
83. Lee, C.S.; Conradie, A.V.; Lester, E. Review of supercritical water gasification with lignocellulosic real biomass as the feedstocks: Process parameters, biomass composition, catalyst development, reactor design and its challenges. *Chem. Eng. J.* **2021**, *415*, 128837. [[CrossRef](#)]
84. Cao, C.; Zhang, Y.; Cao, W.; Jin, H.; Guo, L.; Huo, Z. Transition metal oxides as catalysts for hydrogen production from supercritical water gasification of glucose. *Catal. Lett.* **2017**, *147*, 828–836. [[CrossRef](#)]
85. Cao, C.; Xie, Y.; Chen, Y.; Lu, J.; Shi, J.; Jin, H.; Wang, S.; Zhang, L. Hydrogen production from supercritical water gasification of lignin and cellulose with coprecipitated CuO–ZnO and Fe₂O₃–Cr₂O₃. *Ind. Eng. Chem. Res.* **2021**, *60*, 7033–7042. [[CrossRef](#)]
86. Cao, C.; Xie, Y.; Li, L.; Wei, W.; Jin, H.; Wang, S.; Li, W. Supercritical water gasification of lignin and cellulose catalyzed with co-precipitated CeO₂-ZrO₂. *Energy Fuels* **2021**, *35*, 6030–6039. [[CrossRef](#)]
87. Onwudili, J.A. Supercritical water gasification of RDF and its components over RuO₂/γ-Al₂O₃ catalyst: New insights into RuO₂ catalytic reaction mechanisms. *Fuel* **2016**, *181*, 157–169. [[CrossRef](#)]
88. Samiee-Zafarghandi, R.; Karimi-Sabet, J.; Abdoli, M.A.; Karbassi, A. Supercritical water gasification of microalga *Chlorella* PTCC 6010 for hydrogen production: Box-Behnken optimization and evaluating catalytic effect of MnO₂/SiO₂ and NiO/SiO₂. *Renew. Energy* **2018**, *126*, 189–201. [[CrossRef](#)]
89. Borges, A.C.P.; Onwudili, J.A.; Andrade, H.M.C.; Alves, C.T.; Ingram, A.; Vieira de Melo, S.A.B.; Torres, E.A. Catalytic supercritical water gasification of eucalyptus wood chips in a batch reactor. *Fuel* **2019**, *255*, 115804. [[CrossRef](#)]
90. Borges, A.C.P.; Onwudili, J.A.; Andrade, H.; Alves, C.; Ingram, A.; Vieira de Melo, S.; Torres, E. Catalytic properties and recycling of NiFe₂O₄ catalyst for hydrogen production by supercritical water gasification of eucalyptus wood chips. *Energies* **2020**, *13*, 4553. [[CrossRef](#)]
91. Safari, F.; Javani, N.; Yumurtaci, Z. Hydrogen production via supercritical water gasification of almond shell over algal and agricultural hydrochars as catalysts. *Int. J. Hydrogen Energy* **2018**, *43*, 1071–1080. [[CrossRef](#)]
92. Kumar, A.; Reddy, S.N. Subcritical and supercritical water in-situ gasification of metal (Ni/Ru/Fe) impregnated banana pseudostem for hydrogen rich fuel gas mixture. *Int. J. Hydrogen Energy* **2020**, *45*, 18348–18362. [[CrossRef](#)]
93. Nanda, S.; Reddy, S.N.; Dalai, A.K.; Kozinski, J.A. Subcritical and supercritical water gasification of lignocellulosic biomass impregnated with nickel nanocatalyst for hydrogen production. *Int. J. Hydrogen Energy* **2016**, *41*, 4907–4921. [[CrossRef](#)]
94. Osada, M.; Yamaguchi, A.; Hiyoshi, N.; Sato, O.; Shirai, M. Gasification of sugarcane bagasse over supported ruthenium catalysts in supercritical water. *Energy Fuels* **2012**, *26*, 3179–3186. [[CrossRef](#)]
95. Taylor, A.D.; DiLeo, G.J.; Sun, K. Hydrogen production and performance of nickel based catalysts synthesized using supercritical fluids for the gasification of biomass. *Appl. Catal. B Environ.* **2009**, *93*, 126–133. [[CrossRef](#)]

96. Yamaguchi, A.; Hiyoshi, N.; Sato, O.; Bando, K.K.; Osada, M.; Shirai, M. Hydrogen production from woody biomass over supported metal catalysts in supercritical water. *Catal. Today* **2009**, *146*, 192–195. [[CrossRef](#)]
97. Wang, Y.; Zhu, Y.; Liu, Z.; Wang, L.; Xu, D.; Fang, C.; Wang, S. Catalytic performances of Ni-based catalysts on supercritical water gasification of phenol solution and coal-gasification wastewater. *Int. J. Hydrogen Energy* **2019**, *44*, 3470–3480. [[CrossRef](#)]
98. Rashidi, M.; Tavasoli, A. Hydrogen rich gas production via supercritical water gasification of sugarcane bagasse using unpromoted and copper promoted Ni/CNT nanocatalysts. *J. Supercrit. Fluids* **2015**, *98*, 111–118. [[CrossRef](#)]
99. de Vlieger, D.J.M.; Thakur, D.B.; Lefferts, L.; Seshan, K. Carbon nanotubes: A promising catalyst support material for supercritical water gasification of biomass waste. *ChemCatChem* **2012**, *4*, 2068–2074. [[CrossRef](#)]
100. Huang, J.; Zhu, C.; Lian, X.; Feng, H.; Sun, J.; Wang, L.; Jin, H. Catalytic supercritical water gasification of glucose with in-situ generated nickel nanoparticles for hydrogen production. *Int. J. Hydrogen Energy* **2019**, *44*, 21020–21029. [[CrossRef](#)]
101. Kumar, A.; Reddy, S.N. In situ sub- and supercritical water gasification of nano-nickel (Ni²⁺) impregnated biomass for H₂ production. *Ind. Eng. Chem. Res.* **2019**, *58*, 4780–4793. [[CrossRef](#)]
102. Shen, Y.; Zhao, P.; Shao, Q.; Takahashi, F.; Yoshikawa, K. In situ catalytic conversion of tar using rice husk char/ash supported nickel–iron catalysts for biomass pyrolytic gasification combined with the mixing-simulation in fluidized-bed gasifier. *Appl. Energy* **2015**, *160*, 808–819. [[CrossRef](#)]
103. Fougere, D.; Nanda, S.; Clarke, K.; Kozinski, J.A.; Li, K. Effect of acidic pretreatment on the chemistry and distribution of lignin in aspen wood and wheat straw substrates. *Biomass Bioenergy* **2016**, *91*, 56–68. [[CrossRef](#)]
104. Sun, J.; Xu, L.; Dong, G.H.; Nanda, S.; Li, H.; Fang, Z.; Kozinski, J.A.; Dalai, A.K. Subcritical water gasification of lignocellulosic wastes for hydrogen production with Co modified Ni/Al₂O₃ catalyst. *J. Supercrit. Fluids* **2020**, *162*, 104863. [[CrossRef](#)]

Disclaimer/Publisher’s Note: The statements, opinions and data contained in all publications are solely those of the individual author(s) and contributor(s) and not of MDPI and/or the editor(s). MDPI and/or the editor(s) disclaim responsibility for any injury to people or property resulting from any ideas, methods, instructions or products referred to in the content.